JOURNAL OF GEOPHYSICAL RESEARCH, VOL. 114, A12310, doi:10.1029/2009JA014711, 2009

Steep, transient density gradients in the Martian ionosphere similar to the ionopause at Venus

F. Duru,[1] D. A. Gurnett,[1] R. A. Frahm,[2] J. D. Winningham,[2]
D. D. Morgan,[1] and G. G. Howes[1]

Received 30 July 2009; revised 25 August 2009; accepted 1 September 2009; published 15 December 2009.

[1] With the Mars Advanced Radar for Subsurface and Ionospheric Sounding (MARSIS) on the Mars Express (MEX) spacecraft, the electron density can be measured by two methods: from the excitation of local plasma oscillations and from remote sounding. A study of the local electron density versus time for 1664 orbits revealed that in 132 orbits very sharp gradients in the electron density occurred that are similar to the ionopause boundary commonly observed at Venus. In 40 of these cases, remote sounding data have also confirmed identical locations of steep ionopause-like density gradients. Measurements from the Analyzer of Space Plasma and Energetic Atoms (ASPERA-3) electron spectrometer and ion mass analyzer instruments (also on Mars Express) verify that these sharp decreases in the electron density occur somewhere between the end of the region where ionospheric photoelectrons are dominant and the magnetosheath. Combined studies of the two experiments reveal that the steep density gradients define a boundary where the magnetic fields change from open to closed. This study shows that, although the individual cases are from a wide range of altitudes, the average altitude of the boundary as a function of solar zenith angle is almost constant. The average altitude is approximately 500 km up to solar zenith angles of 60°, after which it shows a slight increase. The average thickness of the boundary is about 22 km according to remote sounding measurements. The altitude of the steep gradients shows an increase at locations with strong crustal magnetic fields.

Citation: Duru, F., D. A. Gurnett, R. A. Frahm, J. D. Winningham, D. D. Morgan, and G. G. Howes (2009), Steep, transient density gradients in the Martian ionosphere similar to the ionopause at Venus, *J. Geophys. Res.*, *114*, A12310, doi:10.1029/2009JA014711.

1. Introduction

[2] Mars Advanced Radar for Subsurface and Ionospheric Sounding (MARSIS) is a low-frequency radar carried by the Mars Express (MEX) spacecraft, which was placed in an elliptical orbit around Mars on 25 December 2003 [*Chicarro et al.*, 2004]. MARSIS is designed to perform both subsurface and ionospheric soundings [*Picardi et al.*, 2004]. One capability of the ionospheric sounding mode of MARSIS is the measurement of the plasma frequency near the Mars Express spacecraft (the local plasma frequency) by means of detecting local plasma oscillations. In this paper, we exploit this capability to demonstrate the existence of steep gradients in the electron density at Mars, similar to the ionopause boundary that is commonly observed at Venus. We confirm the nature of the feature detected by comparing our results with the data from the Analyzer of Space Plasma and Energetic Atoms (ASPERA-3), the plasma detector aboard MEX.

[3] MARSIS consists of a 40 m tip-to-tip dipole antenna, a 7 m monopole antenna, a radio transmitter, a receiver, and a digital signal processing system [*Picardi et al.*, 2004]. Prior to MARSIS, information about the ionosphere of Mars was gathered mostly by using the radio occultation technique [*Kliore et al.*, 1965; *Fjeldbo et al.*, 1966; *Zhang et al.*, 1990; *Luhmann and Brace*, 1991; *Kliore*, 1992; *Hinson et al.*, 2001; *Pätzold et al.*, 2005], which is based on measurements of the phase shift of a radio signal from a spacecraft as it is occulted by the ionosphere of a planet [*Schunk and Nagy*, 2000]. Radio occultation measurements did not provide clear evidence of an ionopause boundary in the electron density at Mars [*Nagy et al.*, 2004]. The Mars Global Surveyor (MGS), which carried a magnetometer, an electron reflectometer, and a radio science investigation, provided important information about the solar wind interaction with the upper atmosphere of Mars [*Brain*, 2006]. According to the MGS radio occultation experiment, when crustal magnetic field effects are excluded, solar wind interaction with Mars is similar to that of Venus [*Cloutier et al.*, 1999].

[4] The MARSIS ionospheric sounding mode provides electron density measurements from the ionosphere of Mars by using two techniques. The remote sounding technique, which provides electron density measurements in the alti-

[1]Department of Physics and Astronomy, University of Iowa, Iowa City, Iowa, USA.
[2]Southwest Research Institute, San Antonio, Texas, USA.

0148-0227/09/2009JA014711$09.00

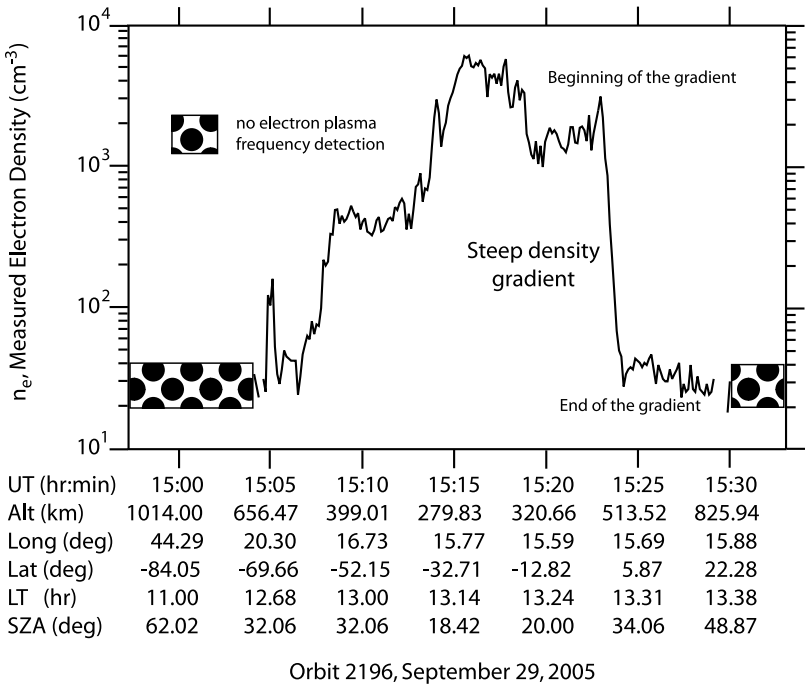

Figure 1. The electron density versus UT profile of a for a 36 min pass on 29 September 2005. A very sharp decrease in the electron density is observed at 1523 UT, at an altitude of 419 km and SZA of 28°. Plasma oscillations are not observed from the beginning of the pass at 1457 UT until 1504 UT, where they suddenly appear. Similarly, electron plasma oscillations suddenly disappear at about 1530 UT until the end of the pass. The sudden appearance and disappearance of the electron plasma oscillations are attributed to the high flow velocity of the shocked solar wind.

tude range between 130 and 400 km, involves sending a short radio pulse of frequency f and measuring the time delay of the returning echo. This method uses the assumption that the ionosphere has constant density at constant altitude (i.e., it is horizontally stratified) and therefore the wave is reflected vertically [*Gurnett et al.*, 2005]. The second method, which provides electron densities from much higher altitudes, between 275 and 1300 km, is from the excitation of local electron plasma oscillations. In the ionospheric sounding mode, when the transmitter frequency is near the local electron plasma frequency, electron plasma oscillations are excited at the local electron plasma frequency. Because these oscillations are usually very intense, harmonics of the basic oscillation frequency are introduced in the detector. Ionograms, which are plots of echo intensity as a function of frequency and time delay, are often used to display the MARSIS data. Electron plasma oscillation harmonics are seen as equally spaced vertical lines at low frequencies (*Duru et al.* [2008, Figure 2] provides an ionogram displaying electron plasma oscillation harmonics). When the plasma frequency is below the 100 kHz low-frequency limit of the receiver, the fundamental of the electron plasma frequency cannot be observed. However, the electron plasma frequency can still be determined by measuring the spacing between the harmonics. Once the electron plasma frequencies are obtained, corresponding electron densities can be calculated using the formula $n_e = (f_p/8980)^2$, where the electron density, n_e, is in cm^{-3} and electron plasma frequency, f_p, is in Hz [*Gurnett and Bhattacharjee*, 2005]. The use of electron plasma oscillations by MARSIS to measure the local plasma frequency, along with results from this method, is discussed by *Gurnett et al.* [2005] and *Duru et al.* [2008].

[5] In this study, we shall compare results from local plasma oscillation measurements with plasma observations made by ASPERA-3 aboard MEX. ASPERA-3 is designed to study the plasma and neutral gas environment in near-Mars space, including the interaction between the solar wind and the atmosphere of Mars. The ASPERA-3 instrument consists of an electron spectrometer (ELS); an ion mass analyzer (IMA); and a main unit consisting of a neutral particle imager, a neutral particle detector, and a digital processing unit, all mounted on top of a scan platform, except for IMA [*Barabash et al.*, 2004]. The ELS is an ultralight, low-power electron sensor, with a field of view of 360° × 4° and an electron energy range up to 20 keV/q [*Frahm et al.*, 2006].

[6] The IMA contains an elevation analyzer, electrostatic top hat deflection, and a magnetic velocity filter that is segmented like an orange. The elevation analyzer provides the view of up to ±45° in 16 steps of elevation, or roughly every 5.6°. The electrostatic top hat deflection filters energies from 0.01 to 30 keV/q and allows a 360° view in 16 segments, i.e., every 22.5° of azimuth. The segmented style of magnetic filter provides momentum analysis, allowing a mass spectrum up to about 40 amu to be determined [*Barabash et al.*, 2006].

2. Description of the Steep Density Gradients

[7] An example of a steep density gradient similar to the ionopause of Venus is shown in Figure 1. In this pass from

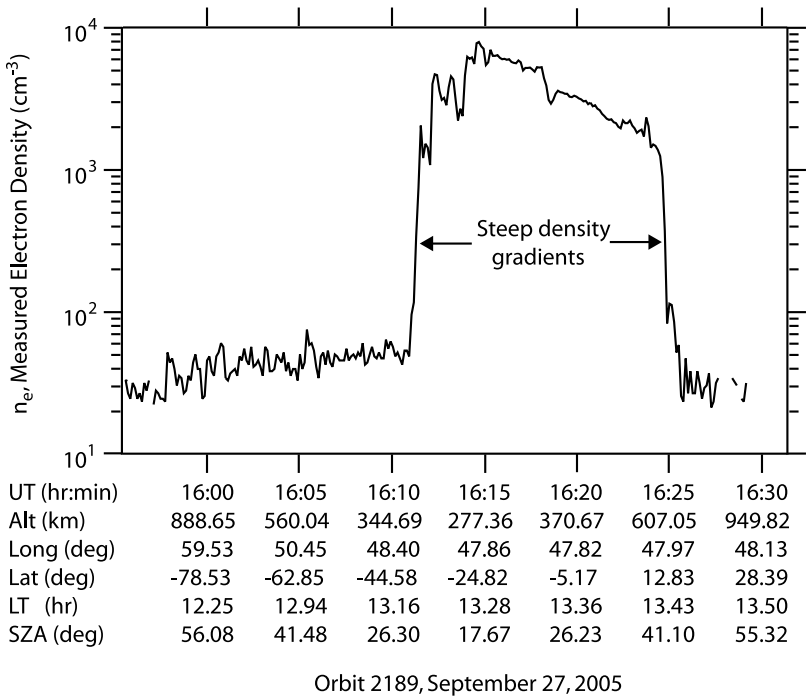

Figure 2. Another plot of electron density versus UT for a 36 min pass on 27 September 2005. This is one of the few cases where a steep density gradient is identified on both legs of the pass. The first sharp electron density drop is seen at 1611 UT, at an altitude of 313 km and SZA of 22.39°. The second one is observed at 1624 UT, at an altitude of 565 km and SZA of 38.2°.

29 September 2005, the electron density in cm^{-3} is presented on the vertical axis, and the horizontal axis shows the universal time (UT), altitude (Alt), longitude (Long), latitude (Lat), local time (LT), and solar zenith angle (SZA). The pass starts at around 1457 UT and ends around 1533 UT. For the first 7 min, electron plasma oscillations are not detected; therefore, it is not possible to obtain the local electron densities. The same situation occurs starting from 1530 UT to the end of the pass. Possible reasons for the disappearance of the electron plasma oscillations are stated by *Duru et al.* [2008] and studied extensively by *Duru et al.* [2009]. They concluded that high flow velocity (above ∼160 km/s) of the shocked solar wind plasma carries the wave packet away from the receiver before the plasma oscillation can be detected [*Duru et al.*, 2009]. After the first detection of the electron plasma oscillations at around 1504 UT, the electron density increases with decreasing altitude up to about 1515 UT, where the altitude starts to decrease. The electron density profile is characterized by large fluctuations, which are studied in detail by *Gurnett et al.* [2009]. The crucial feature of this pass is that a very sharp drop (compared with the more gradual gradient on the inbound leg) in the electron density is observed at about 1523 UT. These sharp drops in the ionospheric thermal plasma density are commonly seen at Venus and are identified as the ionopause [*Schunk and Nagy*, 2000; *Brace et al.*, 1980]. For instance, *Knudsen et al.* [1979] defined the ionopause at Venus as the altitude above which the electron density first drops below ∼100 cm^{-3}. Here the electron density, which is 3087 cm^{-3}, decreases to 27 cm^{-3} in about 1 min. The beginning of this steep gradient feature is located at an altitude of 419 km and at an SZA of 28°.

[8] In the ionosphere of Venus, steep density gradients, characteristic of an ionopause, are seen often and are usually observed on both the inbound and the outbound legs of a given pass [*Brace et al.*, 1980]. At Mars it was possible to identify only a few passes in which a steep gradient was seen on both legs. Figure 2 shows one of these cases. Figure 2 is a 36 min pass from 27 September 2005, shown in the same format as Figure 1. In this pass, electron plasma oscillations are immediately detected at about 1555 UT and they end at about 1629 UT, only a few minutes before the end of the pass. Two very sharp electron density gradients are seen at about 1611 UT and 1624 UT. In the first case (at 1611 UT), the electron density increases from 48 to 2004 cm^{-3}. In the second case (at 1624 UT) the electron density decreases from 1442 to 81 cm^{-3}. These dramatic changes in the density occur in less than 40 s. The altitudes and SZA values for the two locations are 313 km and 22.39° and 565 km and 38.2°, respectively. The big difference in the altitude of these features at the ends of this pass can be attributed, at least partly, to the effect of the crustal magnetic fields. The steep density gradient crossing at the time showing a higher altitude (1624 UT) occurs in a region with stronger crustal magnetic fields than those of the crossing at lower altitude (1611 UT). The possible effect of the crustal magnetic fields is studied later in this paper.

[9] Compared to those observed for Venus, sharp density steps are rarely seen as often for Mars. Investigation of the profiles of electron density versus UT for 1664 orbits between 4 August 2005 and 16 January 2008 provided only 216 cases in which a sharp electron density gradient was observed. Because any given orbit has an inbound and an outbound leg, the cases where we see a sharp decrease in the

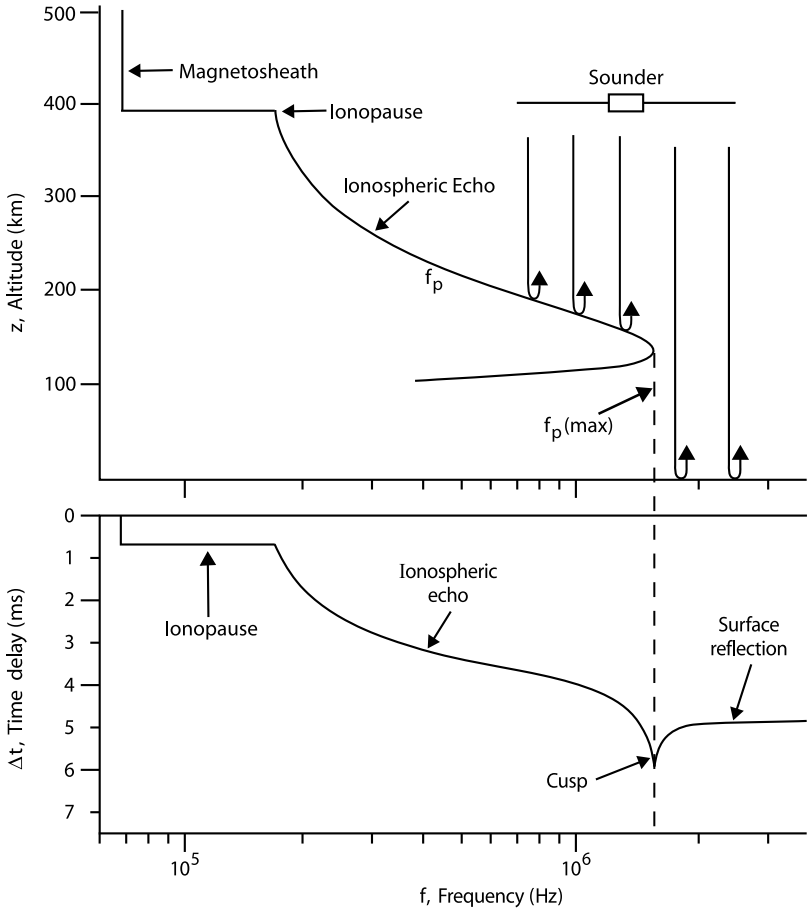

Figure 3. (top) A representative electron plasma frequency profile as a function of the altitude that shows what an ionopause should look like and (bottom) the corresponding MARSIS ionogram. The vertical line at low frequencies is the magnetosheath, which is followed by a short horizontal line at the ionopause. The ionospheric reflection starts after the ionopause and ends at the maximum frequency, after which the surface reflection is observed.

electron density account for only 6.5% of the total number of cases. However, many of the orbits studied (1071 of them) have only about 5 min of data on both sides of the pass. Even if we choose to neglect those half passes, the percentage increases only to 18%. Still, the steep density gradients are not observed in most orbits. After identifying the 216 cases, we applied some filtering criteria to obtain the best cases. We based our criteria on three characteristics: (1) the electron density at the beginning of the density gradient (e.g., 3087 cm^{-3} in Figure 1), (2) the electron density at the end of the density gradient (e.g., 27 cm^{-3} in Figure 1), and (3) the slope of the decrease. After examining many cases, we decided to exclude cases where (1) the electron density at the beginning of the gradient is lower than 500 cm^{-3}, (2) the electron density at the end of the drop is higher than 200 cm^{-3}, and (3) the slope is less than 50 cm^{-3} in the 7.54 s sweep period of the ionospheric sounding. After all the eliminations, 132 boundary points were left for a more detailed study.

3. Observations Through Remote Sounding

[10] Next, we investigate the steep density gradients with the remote sounding data because remote sounding provides a much better spatial resolution than local plasma density measurements. Figure 3 shows what a Venus-like ionopause would look like in an MARSIS ionogram. Figure 3 (top) presents a schematic representation of the electron plasma frequency (f_p) profile as a function of the altitude (h) in the Martian ionosphere. Figure 3 (bottom) shows the corresponding ionogram. The vertical lines at very low frequencies represent the magnetosheath, where the frequency is almost constant over a large range of altitudes. The wave at this frequency is too low to penetrate into the ionosphere. The horizontal lines at low frequencies represent a Venus ionopause-like steep density gradient, where the time delay of the returning echo is nearly constant for the frequencies up to that frequency that passes into the ionosphere. Between the end of the gradient and the maximum frequency in the ionosphere, f_p(max), the normal ionospheric echo is observed. Increasing delay times are observed as the wave frequency is increased. When a critical frequency, f_p(max), is reached, the wave penetrates past the ionization peak in the ionosphere and reflects from the planet's surface. At frequencies greater than f_p(max), the surface reflection may be detected. As can be seen from Figure 3 (bottom), a cusp may be formed between the ionospheric echo and surface reflection.

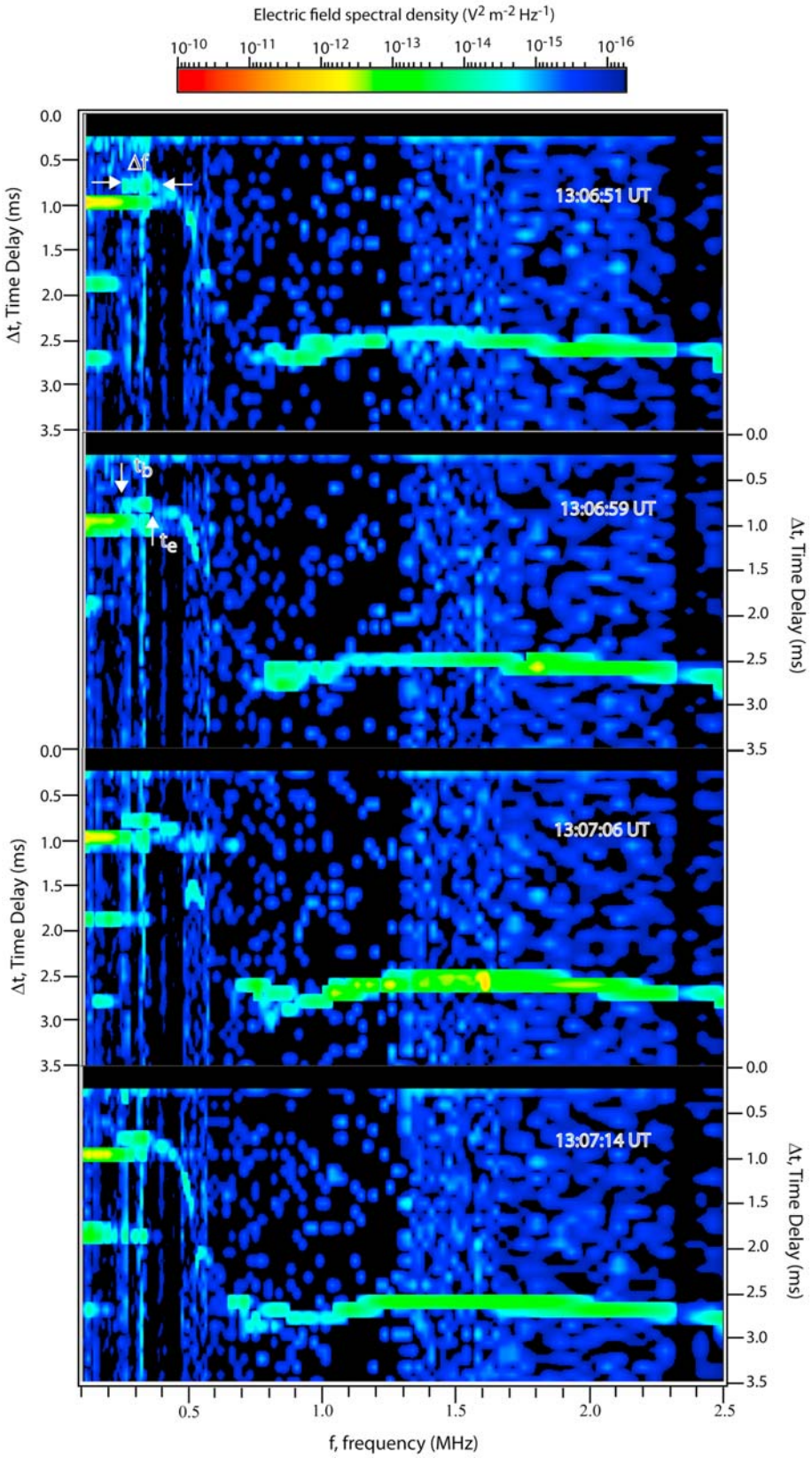

Figure 4. Four consecutive ionograms for the pass from 14 November 2005. The color bar provides the echo intensity. The x and y axes are for the time delay and frequency, respectively. In all the ionograms, the steep density gradient is seen as the horizontal line at low frequencies and low time delays. The variation in frequency across the steep gradient is given by Δf (first panel). The time delay at the beginning (t_b) and end (t_e) of the steep density gradient is shown in the second panel.

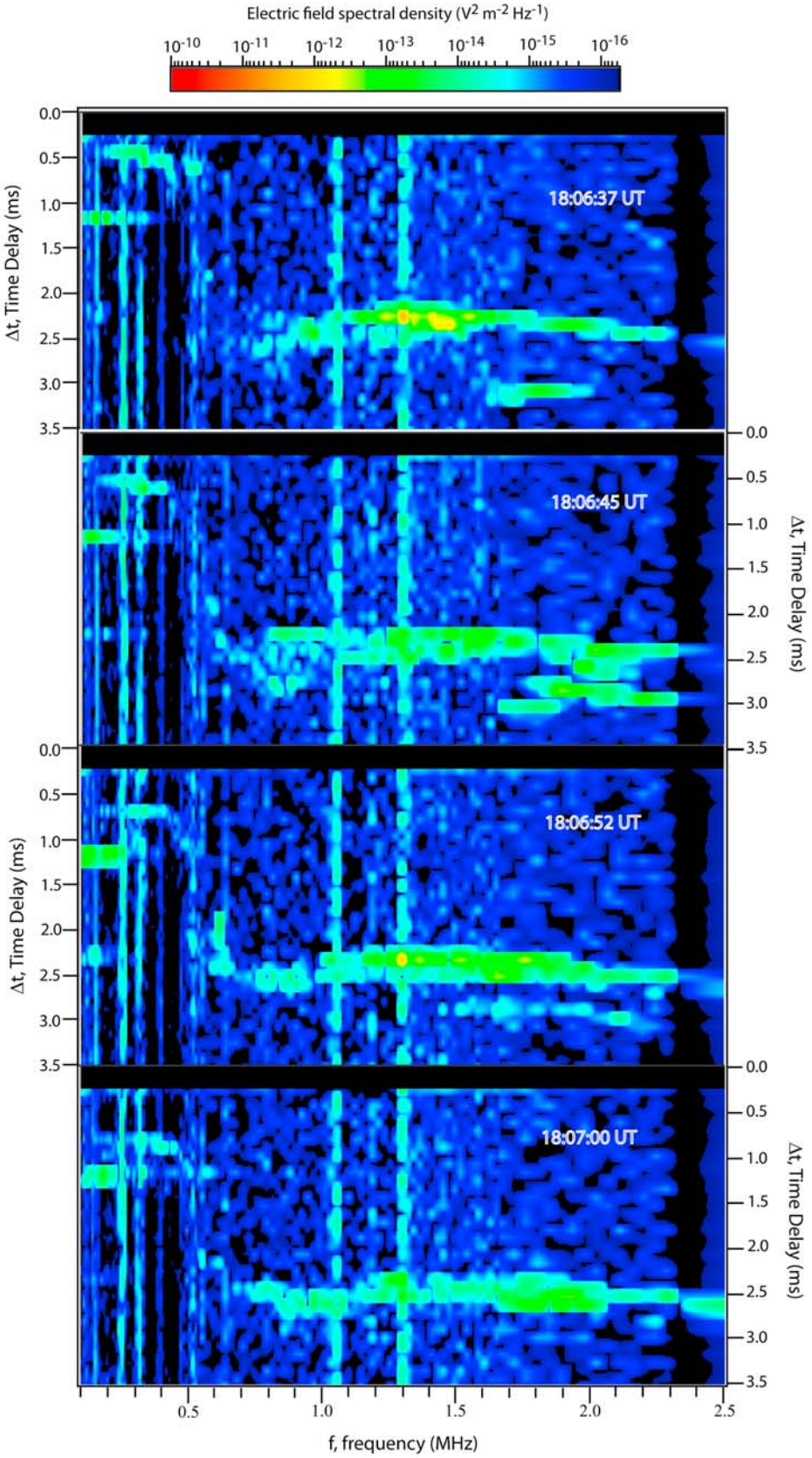

Figure 5. Four consecutive ionograms, this time for the pass on 21 October 2005. Again, the ionogram signature of a steep density gradient is seen as the horizontal line at low frequencies and low time delays.

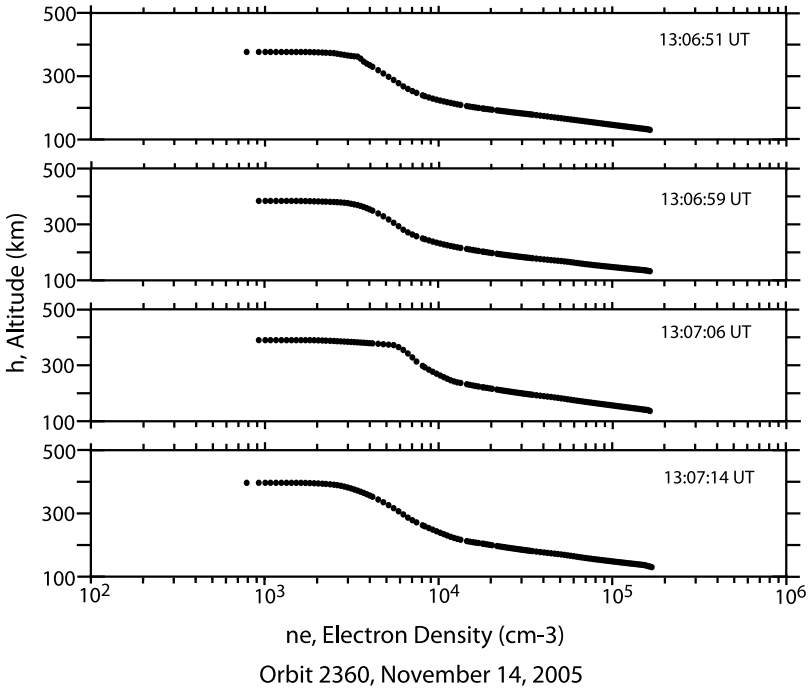

Figure 6. Electron density profile as a function of the altitude for the four ionograms from the same pass as shown in Figure 4 (14 November 2005) obtained by using the inversion technique. The steep density gradient is given by the almost horizontal lines at lower frequencies. The altitude of the gradient, about 390 km, does not vary from ionogram to ionogram.

[11] In Figure 4 we show four consecutive ionograms from an orbit on 14 November 2005 that exhibit the pattern displayed schematically in Figure 3. They are separated by 7.54 s, which is the repetition time of the ionospheric sounding. As expected, the steep gradient in n_e is represented by a horizontal line at low frequencies (<0.5 MHz in this case), indicating a rapid increase in density over a short time range. The longer horizontal line seen at around 2.5 ms

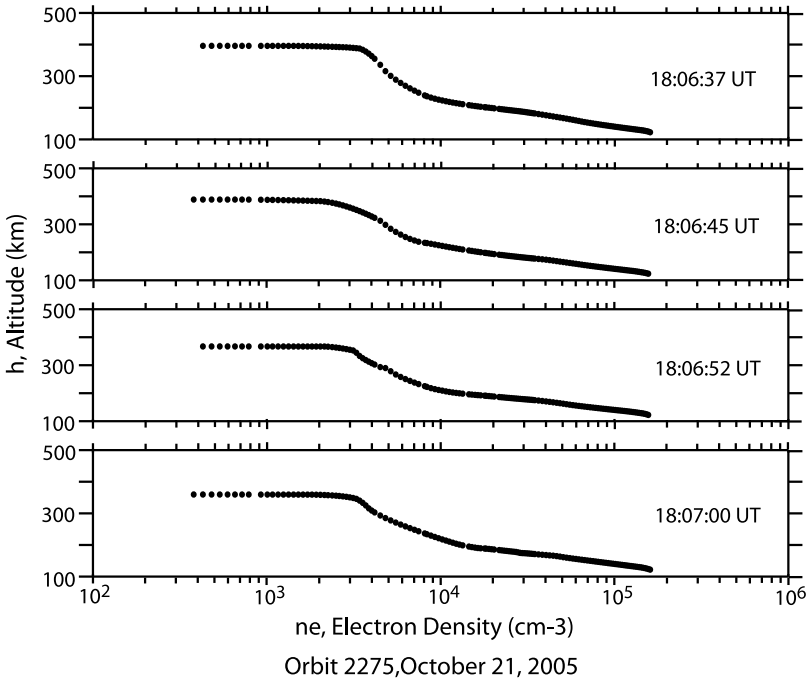

Figure 7. Electron density profile as a function of the altitude for the four ionograms for the same pass as in Figure 5, from 21 October 2005, obtained with the inversion technique. The steep density gradient is given by the almost horizontal lines at lower frequencies. Contrary to Figure 6, the altitude of the gradient changes noticeably.

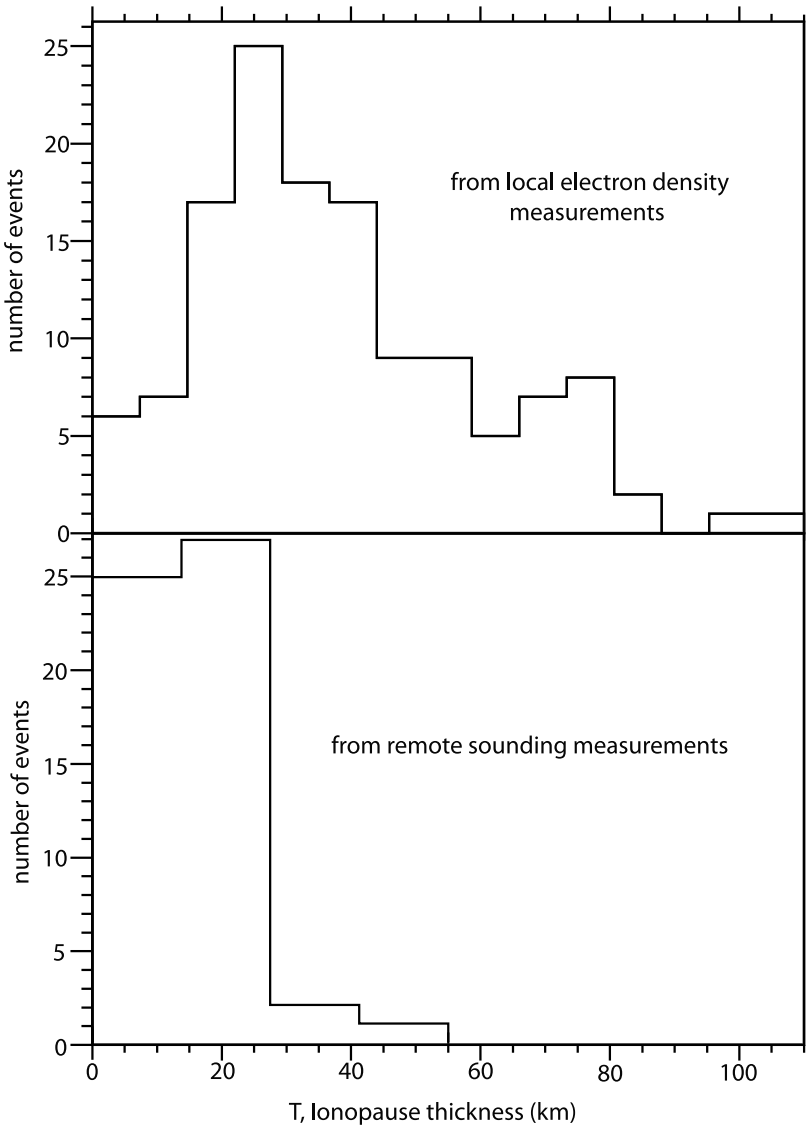

Figure 8. Histograms showing the thickness of the steep density gradients calculated using (top) the local electron density measurements and (bottom) remote sounding measurements. The calculated thicknesses are smaller in the remote sounding case, which is believed to be a more precise computation.

time delay is the reflection from the horizontally stratified ionosphere. All these features are observed through remote sounding. Electron plasma oscillations are not observed in this pass because the spacecraft is out of the ionosphere, possibly in a region with high plasma flow velocity. Also, to give a better view of the steep density gradient, the ionograms are expanded at lower frequencies where surface reflection is not observed. For this pass, the time delay of the steep gradient does not change significantly from ionogram to ionogram. However, the pass shown in Figure 5 on 21 October 2005 gives an example of a steep gradient that varies strongly in time delay. Again, the short, horizontal line at frequencies between about 0.15 and 0.5 MHz is clear. The time delay of this line changes rapidly between $\sim$0.4 and $\sim$0.8 ms within only four ionograms, which corresponds to about 30 s. For the passes shown in Figures 4 and 5, the vertical velocities of the spacecraft are similar. The rapid change in the time delay, seen in the second pass, could be due to either a horizontal spatial gradient or a time variation in the altitude of the density structures caused by a variation in the solar wind pressure.

[12] We have investigated ionograms near the steep gradient locations found from local electron density profiles and have identified 40 passes (out of 132) where we observed the gradients through remote sounding. In many passes, however, the electron plasma frequency harmonics and electron cyclotron echoes prevent us from observing the steep density gradients.

[13] It is possible to obtain the profiles of electron density as a function of the altitude by inverting the frequency dependence of the sounding wave reflection [*Morgan et al.*, 2008]. Figures 6 and 7 show the altitude versus electron density profiles obtained from the inversion technique for the ionograms in Figures 4 and 5, respectively. Here it is assumed that the electron density in the magnetosheath is constant (at 6 cm^{-3} for Figure 6 and at 15 cm^{-3} for Figure 7). These magnetosheath electron density values are estimated according to ASPERA-3 data. In Figures 6 and 7,

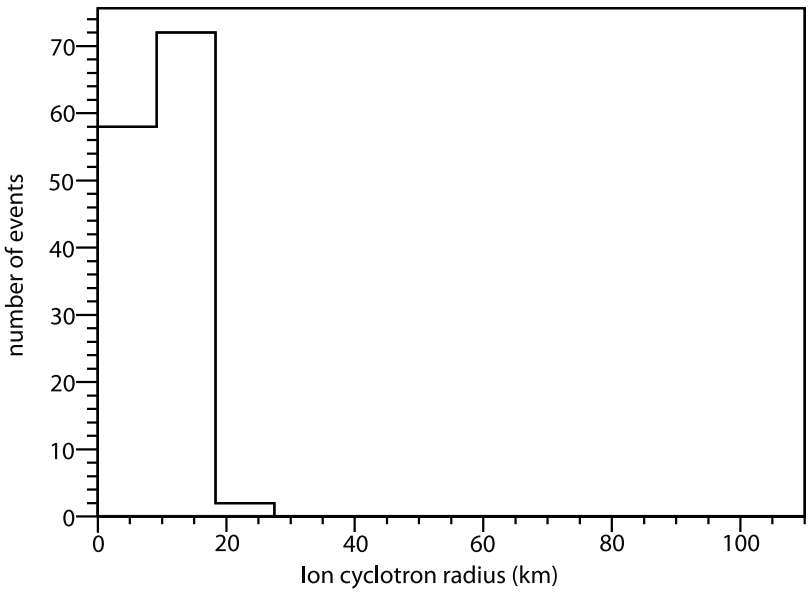

Figure 9. Ion cyclotron radius calculated for every steep density gradient crossing. To make the calculation, it is assumed O_2^+ ions at 3000 K. The distribution is similar to the distribution of the thicknesses calculated using remote sounding measurements.

too, the steep gradient can be seen as the horizontal line at lower frequencies. For the pass in Figure 6, the ionopause altitude is fairly constant around 390 km, whereas for the pass in Figure 7, the altitude starts around 400 km and decreases to 340 km.

4. Thickness of the Steep Density Gradients

[14] We next address the issue of steep density gradient thickness because of its relevance to the physics of the boundary [*Elphic et al.*, 1981]. In this study, thickness is calculated by using two methods. In the first method, the local electron density profiles are used, and the thickness is defined as the altitude difference between the beginning and the end of the sharp electron density drop. The histogram showing the thicknesses thus obtained is displayed in Figure 8 (top). Calculations show that the thickness varies substantially from orbit to orbit. The thickness is as low as 5 km in some cases; however, in other cases the thickness is about 100 km. The mean thickness is calculated to be 37.5 km, with a standard deviation of 20 km. We choose to call this thickness "the apparent thickness" because it is assumed that there are no spatial or temporal variations and that the ionopause boundary is stationary. However, an ionopause-like boundary should move in response to solar wind pressure variations. If so, extracting spatial information requires knowledge of the velocity of the boundary (v_b). Without knowing v_b, one cannot find the actual thickness of the boundary. The spacecraft requires about 1 min to cross the boundary. Although this time interval may seem to be small enough to justify our assumption, it is substantial for an accurate determination of the thickness of the boundary.

[15] The histogram in Figure 8, created with local electron density data, is similar to the one computed by *Elphic et al.* [1981, Figure 4]. They calculated the ionopause thickness for Venus by finding the altitude range corresponding to 90% of the total magnetic field variation observed about the center of the sheet. According to their histogram, the distribution of the thickness has a peak near 30 km, and larger values of thickness are also seen. Their calculation (as in our calculation of the thickness from local electron densities) assumes that the boundary is stationary, which would cause a scatter about the actual values. They also note that boundary waves due to Kelvin-Helmholtz instability can create problems for single-spacecraft analysis. This effect should be most pronounced at high altitudes where boundary motion is more rapid [*Elphic et al.*, 1981].

[16] In the second method, the following equation is used to calculate the thickness from the remote sounding data:

$$\Delta h = \frac{1}{2}\Delta t_i\, c, \tag{1}$$

where Δt_i ($= t_e - t_b$) is the difference between the time delay at the end of the steep density gradient (t_e) and the time delay at the beginning of the steep density gradient (t_b) (see Figure 4) and c is the speed of light ($\sim 3 \times 10^8$ m/s). The factor of 1/2 is used because the time delay is the time required for the pulse to go to and come back from the reflection point.

[17] This method should provide a more precise determination of thickness than the method using local plasma oscillations because an ionogram presents data obtained over only 1.26 s, which is the time it takes to completely scan all the frequencies between 0.1 and 5.5 MHz, as opposed to the 7.54 s resolution of local plasma frequency data. Spatial and temporal effects are therefore much less likely to affect the results in this method. The altitude resolution of the ionograms is about 14 km (91 μs $\times$ $\frac{1}{2}$ $\times$ (3×10^8 m/s), where 91 μs is one time delay bin) with the upper limit of the thickness taken at the calculated value. For instance, if the thickness is calculated to be 28 km, the actual thickness is between 14 and 28 km. This method was applied to 55 ionograms, and the quality of the data did not

Table 1. Number of Cases for Specific Density Change Ranges and Thickness

	Difference in Electron Density Across the Boundary, Δn (cm^{-3})							
Thickness (km)	400–900	900–1400	1400–1900	1900–2400	2400–2900	2900–3400	3400–3900	3900–4400
0–10	3	1	1	2	0	0	0	2
10–20	3	2	4	3	2	0	0	1
20–30	11	9	4	3	3	4	0	0
30–40	11	4	4	1	2	0	1	0
40–50	9	2	3	2	1	1	0	0
50–60	4	2	3	2	0	1	0	0
60–70	2	0	0	0	2	0	0	0
70–80	5	3	4	0	1	0	0	0
80–90	1	0	1	0	0	0	0	0
90–100	0	0	0	0	0	0	0	0
100–110	2	0	0	0	0	0	0	0

allow determination of both t_b and t_e in order to measure the time delay of the ionopause for the remainder of the passes. The results are shown in the histogram in Figure 8 (bottom). The mean value is about 22 km, with a standard deviation of 8.8 km. The comparison of the local density data and remote sounding data shows that the thicknesses obtained from using remote sounding measurements are smaller than those obtained using local electron density measurements. This difference can be attributed to the improved resolution of the remote sounding data eliminating the effect of temporal variations, such as the altitude of the spacecraft and the density gradient, involved in the local density measurements. We believe that the remote sounding data provide a more accurate determination of the boundary thickness than can be obtained from the local measurements.

[18] It is expected that the thickness of the ionopause boundary should scale with the ion cyclotron radius [*Elphic et al.*, 1981]. As a consequence, the thickness and the magnitude of the magnetic field at the ionosphere close to the gradient should be related to each other. To calculate the ion cyclotron radius, we used

$$\rho_c = m(2KT/m)^{1/2}/eB, \tag{2}$$

where m is the mass of the ion, K is the Boltzmann constant, T is the temperature, e is the charge of the electron, and B is the magnitude of the magnetic field. It is assumed that the dominant ion is O_2^+ at a temperature of 3000 K, which is a reasonable choice at the average altitude of the boundary according to Viking data [*Schunk and Nagy*, 2000]. The magnetic field values used in the measurements are derived from electron cyclotron echoes [*Gurnett et al.*, 2005, 2008; *Akalin et al.*, 2009]. This allows the ion cyclotron radius to be obtained for every gradient case from the local electron density measurements (see Figure 9). The ion cyclotron radius varies between 3 and 22 km, with a mean value of 10.31 km and a standard deviation of 4.02 km. The two histograms (Figures 8, bottom, and 9) are similar to each other, supporting the relationship between the thickness of the ionopause and ion cyclotron radius. The fact that the thickness is usually greater than one ion cyclotron radius may be due to the ambipolar potential created by the large temperature difference across the ionosphere-magnetosheath boundary.

[19] We created Table 1 to examine the possible relationship between the thickness and the change in the electron density through the steep density gradients, Δn ($= n_b - n_e$), where n_b is the electron density value at the beginning of the gradient and n_e is the electron density value at the end of the gradient (see Figure 1). Table 1 shows the number of cases for each range of Δn through the steep gradient and of thickness from the local electron density measurements. The thickness is computed from the first technique discussed. According to Table 1, there is no obvious relationship between the thickness and Δn. The electron density changes across the steep density gradients are usually small. Only a few cases exist for large Δn ranges. A similar calculation performed using remote sounding measurements, by finding the frequency change across the steep gradients and converting it to the change in electron density, showed that the electron density values are lower for the remote sounding case. Possibly, because of the noise in the ionograms, the lower and higher ends of the frequency range cannot be measured clearly.

5. ASPERA-3 ELS and IMA Data

[20] This section compares Venus ionopause–like density gradients identified in the MARSIS local electron density data with ASPERA-3 data. Figure 10 shows the MARSIS local electron density and ASPERA-3 ELS data from sector 9 together for the same pass as in Figure 1. Here the color code gives the electron flux at each energy from ELS data, and the solid black line is the local electron density from MARSIS. The ionospheric electron spectrum of Mars contains photoelectron peaks. These peaks, which result from the photoionization of atmospheric gases, are seen as enhancements in the electron flux in the ASPERA-3 spectrograms [*Frahm et al.*, 2006]. In Figure 10, photoelectrons are visible between around 1507 UT and 1524 UT as a narrow-energy enhancement around 20 eV. Magnetosheath plasma, where the shocked solar wind is present [*Schunk and Nagy*, 2000], can be seen between 1455 UT and 1507 UT as the region where electron flux and energy are much higher than in the ionosphere. The halo/strahl is given by the violet region (10^{-5} erg cm^{-2} sr^{-1} s^{-1} eV^{-1} and less) and reaches energies up to 500 eV. Some bursts are seen at the edge of the magnetosheath, starting at 1504 UT. On the inbound leg, the MARSIS density shows a small jump at the magnetosheath plasma (1507 UT). Photoelectrons start at the same time as well. On the outbound leg, however, it looks like there is a gap between the last observation of photoelectron peaks (at 1524 UT) and the start of magnetosheath plasma observations (at 1526 UT). According to

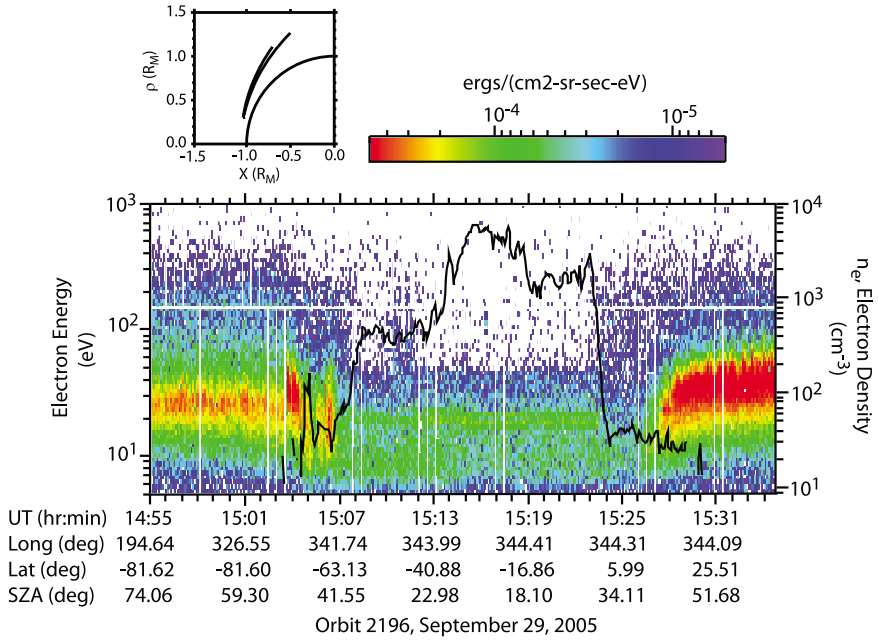

Figure 10. MARSIS and ASPERA-3 ELS data for the same pass as in Figure 1. Color code shows the electron flux, at each energy, from ASPERA-3 ELS, and the solid black line displays local electron density values from MARSIS. On the inbound leg, there is no gap between where the sheath plasma starts and photoelectrons end. A small jump in the electron density is seen when the sheath plasma ends, at around 1507 UT. On the outbound leg, the sharp density drop occurs at the end of the photoelectrons (at 1524 UT), about 2 min before the sheath plasma starts.

Figure 10, the Venus ionopause–like steep density gradient occurs at the end of the photoelectrons. At this time the solar wind's halo/strahl component is observed. However, when the average results from 11 sensors (sectors 1–12) are used to generate a pseudo-omni direction flux, instead of one ELS sector, it is seen that the region that looks like a gap is a transition region where solar wind halo/strahl and ionospheric plasma coexist. Figure 11 shows the ASPERA-3 ELS data for the same pass as in Figure 10, obtained by averaging results from 11 sensors and zooming in to the region where the apparent gap is observed. The first vertical line on the left marks where the solar wind halo/strahl is observed. This corresponds to where the first magnetic field lines open to the solar wind. Before this time, the magnetic field lines are closed and self-sufficient. This place also corresponds to the beginning of the electron density drop determined by MARSIS. The second line is where the electron density drops to a level at which the photoelectron

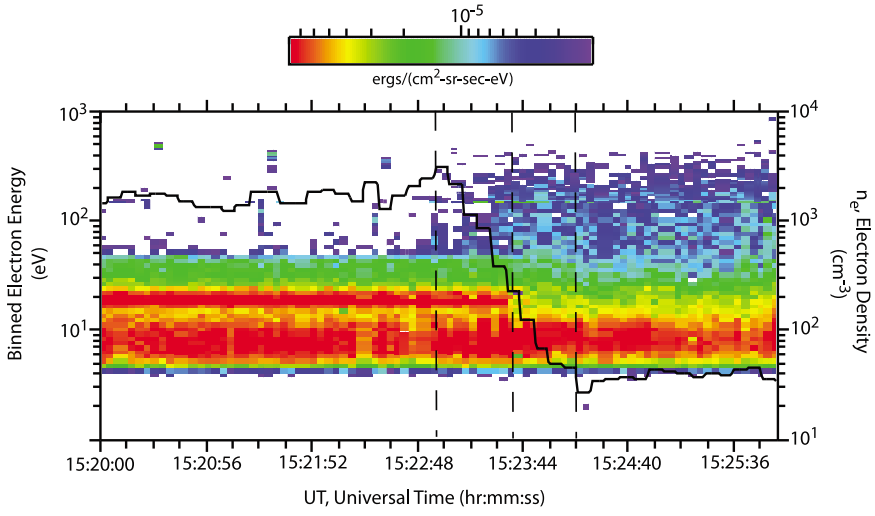

Figure 11. ASPERA-3 ELS data for the pass in Figure 10, which is obtained by averaging data from 11 sensors and zooming at the region where the apparent gap is observed.

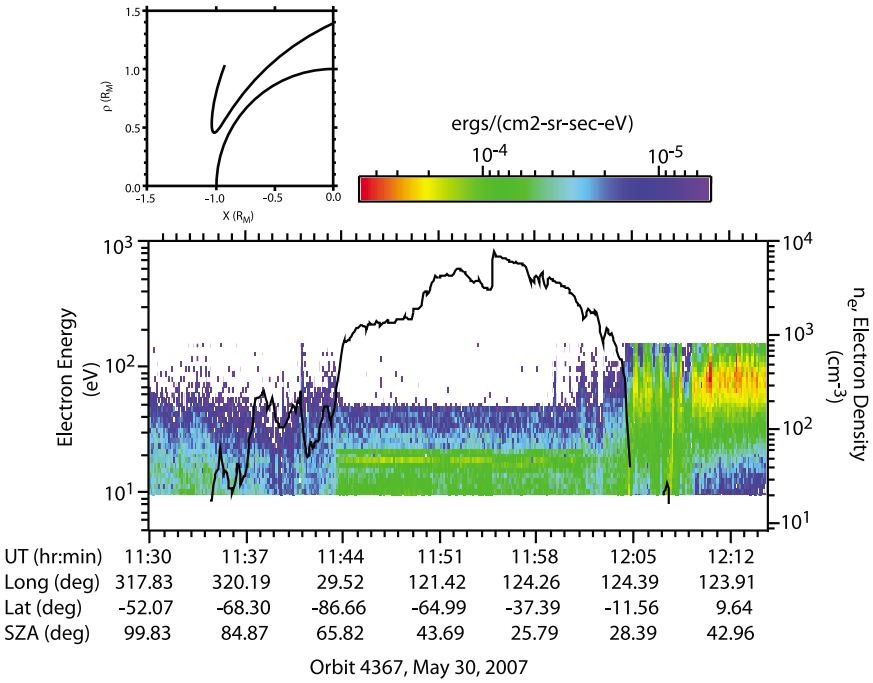

Figure 12. Plot showing MARSIS and ASPERA-3 ELS data together, this time for a 40 min pass from 30 May 2007. This pass starts at 1134:29 UT. A step in the electron density that corresponds to where the photoelectron peak plasma starts is observed at about 1144 UT. On the up leg, steep density gradient occurs about 3 min after the end of the photoelectron peak plasma, at the beginning of the sheath plasma (at an altitude of 575 km and SZA of 27.17°).

peaks are destroyed. After the third line, the only source of electrons is the solar wind. Between the first and third lines, photoelectrons and solar wind electrons are mixed and coexist. According to Figure 11, a change in physical processes is observed at the location, where the Mars atmospheric photoelectrons exhibiting the double-peaked spectra expected for oxygen production are dominant ends and halo/strahl begins to be observed.

[21] As in Figure 10, when the Martian photoelectrons and the sheath plasma are separated by an apparent gap, the steep density gradient has a tendency to occur at the end of the well-defined photoelectron peak. However, at times the gradient occurs at the start of the halo/sheath plasma, such as the case shown in Figure 12. This 40 min pass, from 30 May 2007, starts at 1134:29 UT. At about 1144 UT, there is a step in the electron density that corresponds to where the photoelectrons are first observed. On the upbound leg, the density decreases as the 140 eV plasma intensifies, even though the photoelectrons are observed. The end of the region where photoelectrons are dominant is at about 1201 UT. The very sharp decrease in the electron density occurs about 3 min after this, at the beginning of the magnetosheath plasma. The altitude and SZA where this steep gradient crossing occurs are 575 km and 27.17°, respectively.

[22] In some passes it was possible to obtain good IMA data in addition to ELS data. Figure 13, which is from 10 July 2007, is one of these few passes. Figure 13 (bottom) presents the electron flux from ASPERA-3 ELS data (color coded) and the local electron densities from MARSIS (black line). In this pass, there is almost no apparent gap between the photoelectron boundary and the magnetosheath plasma. However, there is a break in the electron density data between about 0847 UT and 0901 UT because between these times the MARSIS instrument is in subsurface mode and ionospheric sounding is not performed. The density begins after the Martian photoelectrons are observed. The outbound steep gradient is seen at 0914 UT, at the boundary between the photoelectrons and the magnetosheath plasma.

[23] Figure 13 (top) displays the flux of ions from ASPERA-3 IMA data (color coded). Lower-energy heavy ions are observed starting from 0854 UT until the outbound steep gradient, after which higher-energy heavy ions are seen. The black line in Figure 13 (top) shows the magnitude of the magnetic field obtained by MARSIS from electron cyclotron echoes [*Gurnett et al.*, 2005, 2008; *Akalin et al.*, 2009]. In this pass, the magnitude of the magnetic field is fluctuating. Between 0907 and 0908 UT a small decrease in the local electron density and a small electron burst are simultaneously observed. The magnitude of magnetic field decreases starting from 0910 UT but continues even after the ionopause.

[24] In this case, MARSIS local electron density solutions end with the steep gradient. This means that the electron plasma oscillations cannot be detected after the gradient, implying that the flow velocity of the plasma becomes higher than ~160 km/s [*Duru et al.*, 2009] as soon as the spacecraft enters the magnetosheath plasma. This occurs for about 40% of the total cases. For the rest, the electron density is measurable for some distance outside the steep density gradient.

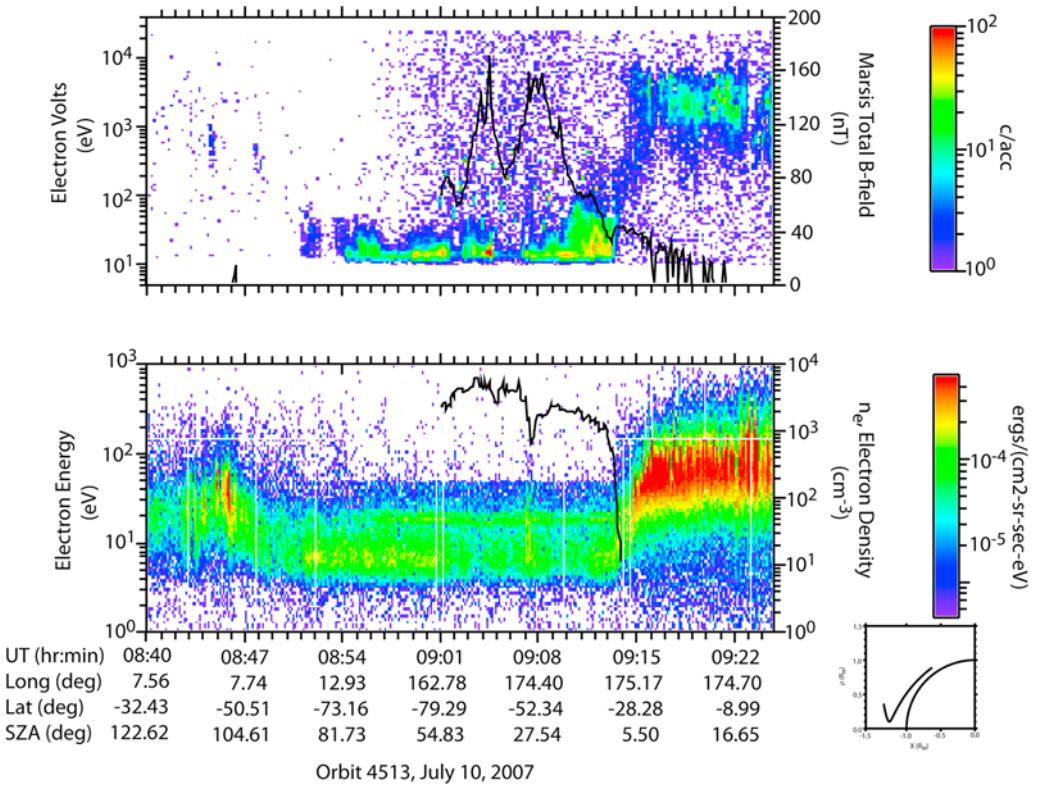

Figure 13. MARSIS, ASPERA-3 ELS, and ASPERA-3 IMA data are shown together for a pass from 10 July 2007. (bottom) Electron flux from ASPERA-3 ELS data (color code) and the local electron densities from MARSIS (black line). (top) Flux of ions from ASPERA-3 IMA data (color code) and the black line shows the magnitude of magnetic field obtained by MARSIS [*Gurnett et al.*, 2005, 2008]. In this pass, there is almost no gap between the photoelectron peak plasma boundary and the sheath plasma. The steep density gradient is observed at 0914 UT, at the boundary between the photoelectron peak plasma and the sheath plasma. Low-energy heavy ions are observed between 0854 UT and the gradient. After the gradient, higher-energy heavy ions are seen.

[25] After observing the ASPERA-3 data, we concluded that the sharp drops in the electron density occur at the boundary between the region where the photoelectrons are dominant and the magnetosheath plasma, i.e., at the boundary of solar wind magnetic field lines, that is, "open" field lines.

6. Location of the Steep Density Gradients

[26] At Venus, the ionopause altitude changes drastically with changing solar wind conditions [*Brace et al.*, 1980]. Therefore, orbit-to-orbit variations in the altitude of the ionopause are widely observed [*Brace et al.*, 1983]. To explore whether similar variations in the ionopause altitude occur at Mars, we investigated all 132 steep density gradients on a Mars map (see Figure 14). In Figure 14, the solid black line is the bow shock from *Trotignon et al.* [2006], and the diamonds are the crossings from MARSIS. The dashed lines indicate the upper and lower limits of the measurements. The crossings are in a large range of altitudes changing between 302 and 979 km; however, most of the crossings lie between about 300 and 600 km. This fact is consistent with the findings of *Schunk and Nagy* [2000], who report a dayside boundary between 300 and 500 km on the basis of Mars Global Surveyor data. There are only seven cases with altitudes above 750 km. These cases, which are marked by small circles in Figure 14, are from all dayside SZAs, longitudes, and latitudes. The only similarity they have is the low (around 500 cm^{-3}) electron density at the beginning of the drop, which could be explained by the high altitude. The upper and lower altitude limits do not vary much with respect to the solar zenith angle. However, as at Venus, the altitude of individual ionopause cases is highly variable.

[27] To find out the average location of the steep density steps in the MARSIS data, we sorted all 132 points according to their SZA. The altitudes are averaged over 10° SZA bins. The result is shown in Figure 15. Here the gray circles are individual crossings and black squares are the average values. The average altitude is 465 km between the subsolar point and 10°. After a small increase between 10° and 20°, the altitude stays almost constant, around 450–500 km until 60°. Between 60° and 70°, the average is high, around 660 km, but it decreases to about 600 km near the terminator. A similar feature is seen at Venus, where a small increase in the altitude is seen with increasing SZA up to 65°, with a maximum at around 85° [*Brace et al.*, 1983]. The increase between 60° and 70° is probably due to the

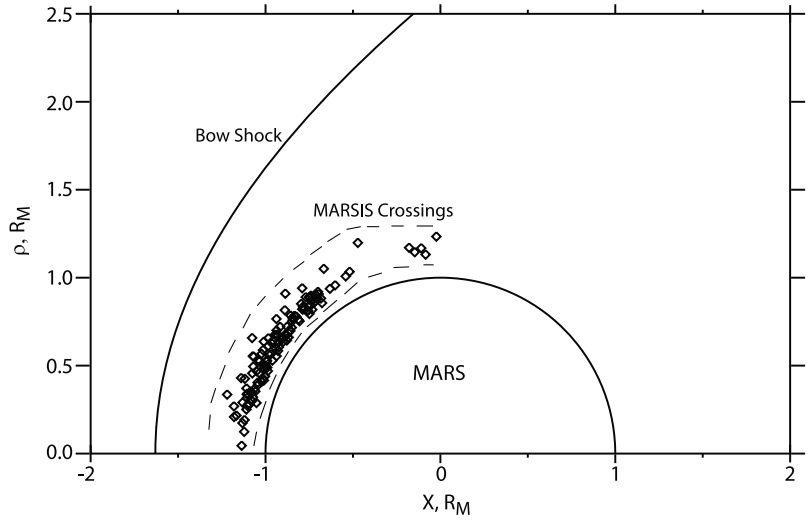

Figure 14. Steep density gradient crossings from MARSIS data (black squares) are shown. The solid black line is the bow shock from *Trotignon et al.* [2006]. The two dashed lines mark the upper and lower limits of the measurements. Most of the MARSIS points lie in an altitude range between 300 and 600 km. The seven points at an altitude higher than 750 km are marked with circles.

few samples in this region; only three crossings are identified between 60° and 70°. No data are available for 70°–80° of SZA range.

7. Crustal Magnetic Field Effect on the Altitude of Steep Density Gradients

[28] That Mars does not have an active dynamo was first deduced from the Mariner 4 data [*Smith et al.*, 1965; *Van Allen et al.*, 1965]. Later, closer MGS flybys of the planet confirmed this result. Instead of a core magnetic field, Mars has strong, small-scale, remnant crustal magnetic fields, which are highly localized [*Acuña et al.*, 1998, 1999; *Ness et al.*, 1999].

[29] The crustal magnetic fields add greatly to the complexity of the ionosphere of Mars and its ionopause [*Nagy et al.*, 2004]. Earlier studies show that the crustal magnetic fields can contribute to irregularities in the ionosphere of Mars [*Gurnett et al.*, 2005; *Duru et al.*, 2006]. They can also affect the electron distribution and have the effect of

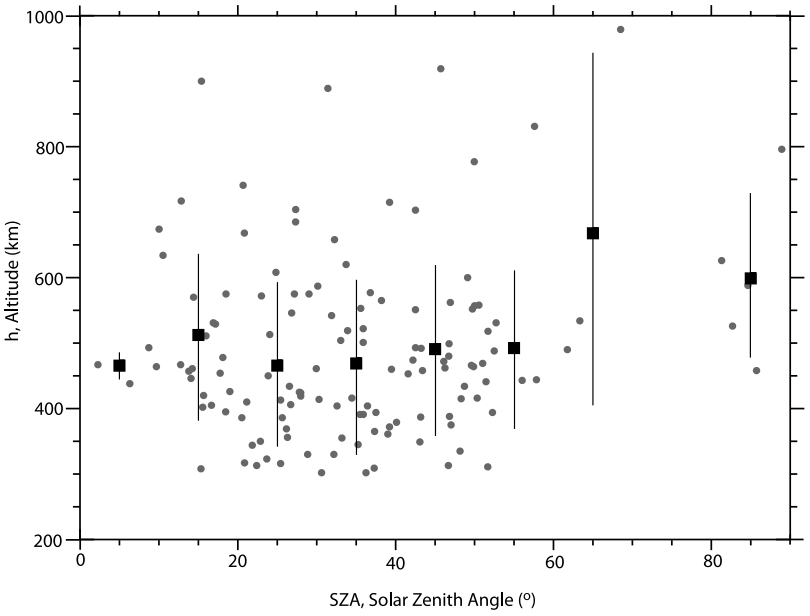

Figure 15. Altitude profile of the steep density gradient boundary as a function of SZA. Small gray dots are the individual crossings. Black squares are obtained by sorting the crossings according to their SZA and averaging their altitudes in 10° SZA bins. Except for some small fluctuations, the average altitude is constant, around 475 km, up to 60°. Between 60° and 70°, the average is high, around 660 km, but it decreases to about 600 km near the terminator.

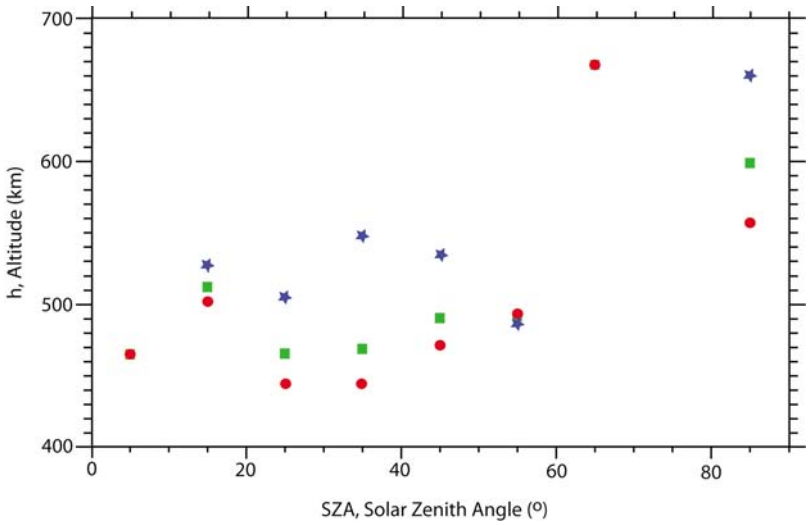

Figure 16. An altitude versus SZA plot showing the effect of crustal magnetic fields on the altitude of the steep gradient boundary. The average boundary altitudes for three different sets of data are shown. Green squares show the average of all the data. Blue stars are for a subset of the data that includes the cases where the crustal magnetic field magnitude is higher than 100 nT at an altitude of 130 km, at the longitude and latitude of the gradient. Red circles are for a subset of the data that includes the cases where the crustal magnetic field magnitude is lower than 100 nT at an altitude of 130 km, at the latitude and longitude of the gradient. The effect of the strong crustal magnetic fields is seen clearly at the SZA range between 10° and 50°, where there the average altitude of boundary is raised.

raising the boundary between Mars' ionosphere and solar wind. By studying the magnetized and unmagnetized regions of Mars, *Crider et al.* [2002] and *Brain et al.* [2005] showed that the strong crustal magnetic fields raise the altitude of magnetic pileup boundary. Similarly, *Duru et al.* [2009] proved that the altitude of the flow velocity boundary is considerably higher at the places where the crustal magnetic fields are strong.

[30] In this study, we used an approach similar to that of *Duru et al.* [2009] to investigate the effect of the crustal magnetic fields on the altitude of the steep density gradient. Using the model of *Cain et al.* [2003], we evaluated the magnitude of the magnetic field at an altitude of 130 km at the latitude and longitude of each ionopause point. The 132 ionopause locations are separated according to the magnitude of the crustal magnetic field. The first group includes the cases having crustal magnetic field magnitude evaluated at 130 km, less than 100 nT, whereas the second group includes the cases with crustal magnetic field magnitude at 130 km, greater than 100 nT.

[31] Figure 16 shows the results of the investigation of crustal magnetic field effect on the altitude of the steep density gradient. The points are obtained by averaging the altitudes of the crossings of each data set over 10° SZA ranges. Green squares show the average altitude of all the data. Blue stars and red circles give the position of the gradient as a function of SZA for the cases where the magnetic field strength is greater than 100 nT and less than 100 nT, respectively, at 130 km and at the longitude and latitude of the gradient feature. According to Figure 16, the effect of the strong crustal fields is obvious for most of the SZA ranges: the altitude is increased where the crustal magnetic fields are strong. This increase is around 60 km for SZA ranges between 20°–30° and 40°–50° and is around 100 km between 30°–40° and 80°–90°. Between 10° and 20°, the increase in the altitude is only 25 km. The average altitude is decreased slightly for the strong magnetic field case in the range between 50° and 60°. Of 13 crossings in this range, only 3 fall into the category with magnetic field greater than 100 nT at 130 km. The unexpected behavior of the data in this range can be attributed to the poor statistics. No comparison could be made for the SZA ranges between 0° and 10° and 60° and 80° because no cases with crustal magnetic fields higher than 100 nT are present in these ranges.

8. Discussion and Conclusions

[32] MARSIS can provide local electron density measurements in an altitude range between 250 and 1300 km. The study of the thermal electron density profiles at altitudes as high as these can reveal important information about the interactions between the solar wind and ionosphere. Investigation of 1664 MARSIS orbits revealed that in the ionosphere of Mars, very sharp gradients in the electron density can be seen in some passes. Similar steep density drops are seen frequently at Venus and are accepted as the classical definition of an ionopause [*Schunk and Nagy*, 2000]. We identified 216 cases of sharp electron density drops in the MARSIS data. To find the best cases, some criteria are used, and 132 very clear crossings are left for further analysis. In 40 of these cases, very steep density gradients that are comparable to the ionopause boundary observed at Venus are observed with remote sounding data. In the ionograms, these density gradients are seen as horizontal lines, i.e., at constant time delay, at low frequencies.

[33] Ionopause crossings are observed in almost every pass at Venus [*Schunk and Nagy*, 2000]. In contrast to the

case of Venus, we observe a steep density gradient in Mars in only about 18% of the samples studied. This percentage is found by excluding all the half passes, in which we may not observe the gradients because of inadequate sampling. The relative rarity of an observed steep gradient suggests that we are detecting a time- and space-variable phenomenon. Previous work has shown that electron density in the ionosphere of Mars is highly fluctuating [*Gurnett et al.*, 2009; *Duru et al.*, 2008]. This rapid variability in time suggests that the fluctuations are generated by a fluid plasma instability. One possibility is the Kelvin-Helmholtz instability, caused by the velocity shear between the solar wind and the ionosphere [*Gurnett et al.*, 2009].

[34] Comparing MARSIS data with ASPERA-3 ELS and IMA data shows that these sharp gradients occur at the boundary between the region dominated by photoelectrons and magnetosheath plasma. Investigation of the ASPERA-3 data reveals that with changing solar wind pressure the boundary between open and closed magnetic field lines moves in and out and allows an explanation of how at least some of these steep density gradients may be formed. To understand this explanation, one must address how the ELS responds to magnetic topology. When ELS detects electrons that exhibit the features of the solar wind plasma, such as the core, halo, and strahl in the magnetosheath of Mars, it means that the field lines have access to the solar wind and must be connected to the solar wind magnetic field. In the transition regions where the solar wind and photoelectrons from the atmosphere of Mars coexist, the field lines go all the way down to the region of maximum photoproduction. The loss of the solar wind population indicates a disconnection from the solar wind source, and this cessation coincides with the steepest electron density. This finding implies that the field lines are closed to thermal plasma escape, causing electron densities to increase. This, in turn, implies that the field lines are not connected to the solar wind and are internally contained.

[35] Pauses in the inward motion of the boundary of open field lines can explain the steep density gradients. As the solar wind pressure increases, the inward motion brings open magnetic field lines into the dense ionosphere, which allows expulsion of ions to the solar wind to occur. According to ASPERA-3, the region of mixed magnetosheath and photoelectrons shows that the open magnetic field lines penetrate deep into the photoionization region of the Martian ionosphere. As the solar wind pressure decreases, the boundary of open and closed magnetic field lines moves upward. Sometimes the boundary moves to very high altitudes where no measurable photoionization occurs. As field lines close at higher altitudes, with outward motion, the density can increase with refilling from below on these closed magnetic field lines. Because they require a special state that depends on external solar wind conditions, steep density gradients are observed in only a small percentage of the total cases studied. The preceding explanation suggests that when steep density gradients occur, we can define a boundary that is the place where the magnetic field changes from open to closed.

[36] The thickness of the steep density gradient crossings, which may provide important information on the physics of the boundary, is calculated with two techniques. First, we used the local electron density data to calculate the altitude range of the ionopause. This technique, which is similar to the one used by *Elphic et al.* [1981] for Venus, yields a mean thickness of 37.5 km. Wider thicknesses are also commonly observed. However, this method has a weakness: it is based on the assumption that there are no spatial or temporal variations during the time that the spacecraft passes through the steep density gradients, which is about 1 min. Our second technique, using remote sounding measurements, has improved spatial resolution. The thicknesses calculated using remote sounding data are usually smaller than the ones calculated with the first method and have a mean value of 22 km. Calculation of the ion cyclotron radius for each crossing yielded an average of about 10 km. The thickness of the crossings and ion cyclotron radius are expected to scale with each other. The fact that the thickness is usually greater than one ion cyclotron radius may be attributed to the ambipolar potential.

[37] The observed crossings occur over a wide range of altitudes. It is possible that the altitude of the individual crossings changes with changing solar wind conditions, as for Venus' ionopause [*Brace et al.*, 1980]. When the altitudes are averaged over 10° of SZA, however, the altitude where the steep density gradients occur is almost constant at a value between 400 and 500 km up to 65°, where it increases by 200 km. Between 80° and the terminator, the average altitude is calculated to be about 600 km.

[38] The presence of strong crustal magnetic fields has the effect of raising the sharp density boundary, sometimes by more than 100 km from its average position. We have also studied the effect of the crustal magnetic fields on the existence of the steep density gradients. Steep density gradients are present in comparable amounts both in the southern hemisphere, where most of the crustal magnetic field regions are located, and the northern hemisphere, which has few regions of strong crustal magnetic field. The magnitude of the magnetic field at 130 km, at the latitude and longitude location of the steep density gradients, varies between about 3.7 and 655.2 nT, implying that strength of the crustal magnetic fields does not have an obvious effect on the existence of the steep density gradients.

[39] **Acknowledgments.** Research at the University of Iowa was funded by contract 1224107 with the Jet Propulsion Laboratory and at Southwest Research Institute by contract NASW-00003 with Marshall Space Flight Center.

[40] Wolfgang Baumjohann thanks Andrew F. Nagy and Paul Cloutier for their assistance in evaluating this paper.

References

Acuña, M. H., et al. (1998), Magnetic field and plasma observations at Mars: Initial results of the Mars Global Surveyor mission, *Science*, *279*, 1676–1680, doi:10.1126/science.279.5357.1676.

Acuña, M. H., et al. (1999), Global distribution of crustal magnetization discovered by the Mars Global Surveyor MAG/ER experiment, *Science*, *284*, 790–793, doi:10.1126/science.284.5415.790.

Akalin, F., D. D. Morgan, D. A. Gurnett, D. L. Kirchner, D. A. Brain, R. Modolo, M. H. Acuña, and J. R. Espley (2009), Dayside induced magnetic field of the ionosphere of Mars, *Icarus*, doi:10.1016/j.icarus.2009.03.021, in press.

Barabash, S., et al. (2004), ASPERA-3: Analyser of Space Plasmas and Energetic Ions for Mars Express, in *Mars Express: The Scientific Payload*, edited by Andrew Wilson, *Eur. Space Agency Special Publ., ESA SP-1240*, 121–139.

Barabash, S., et al. (2006), The Analyzer of Space Plasmas and Energetic Atoms (ASPERA-3) for the Mars Express Mission, *Space Sci. Rev.*, *126*, 113–164, doi:10.1007/s11214-006-9124-8.

Brace, L. H., R. F. Theis, W. R. Hoegy, J. H. Wolfe, J. D. Mihalov, C. T. Russell, R. C. Elphic, and A. F. Nagy (1980), The dynamic behavior of the Venus ionosphere in response to solar wind interactions, *J. Geophys. Res.*, *85*(A13), 7663–7678, doi:10.1029/JA085iA13p07663.

Brace, L. H., H. A. Taylor Jr., T. I. Gombosi, A. J. Kliore, W. C. Knudsen, and A. F. Nagy (1983), The ionosphere of Venus: Observations and their interpretation, in *Venus*, edited by D. M. Hunten et al., pp. 779–840, Univ. of Ariz. Press, Tucson.

Brain, D. A. (2006), Mars Global Surveyor measurements of the Martian solar wind interaction, *Space Sci. Rev.*, *126*, 77–112, doi:10.1007/s11214-006-9122-x.

Brain, D. A., J. S. Halekas, R. Lillis, D. L. Mitchell, and R. P. Lin (2005), Variability of the altitude of the Martian sheath, *Geophys. Res. Lett.*, *32*, L18203, doi:10.1029/2005GL023126.

Cain, J. C., B. B. Ferguson, and D. Mozzoni (2003), An $n = 90$ internal potential function of the Martian crustal magnetic field, *J. Geophys. Res.*, *108*(E2), 5008, doi:10.1029/2000JE001487.

Chicarro, A., P. Martin, and R. Traunter (2004), Mars Express: A European mission to the red planet, in *Mars Express: The Scientific Payload*, edited by A. Wilson, *Eur. Space Agency Spec. Publ., ESA SP-1240*, 3–16.

Cloutier, P. A., et al. (1999), Venus-like interaction of the solar wind with Mars, *Geophys. Res. Lett.*, *26*(17), 2685–2688, doi:10.1029/1999GL900591.

Crider, D. H., et al. (2002), Observations of the latitude dependence of the location of the Martian magnetic pileup boundary, *Geophys. Res. Lett.*, *29*(8), 1170, doi:10.1029/2001GL013860.

Duru, F., D. A. Gurnett, T. F. Averkamp, D. L. Kirchner, R. L. Huff, A. M. Persoon, J. J. Plaut, and G. Picardi (2006), Magnetically controlled structures in the ionosphere of Mars, *J. Geophys. Res.*, *111*, A12204, doi:10.1029/2006JA011975.

Duru, F., D. A. Gurnett, D. D. Morgan, R. Modolo, A. Nagy, and D. Najib (2008), Electron densities in the upper ionosphere of Mars from the excitation of electron plasma oscillations, *J. Geophys. Res.*, *113*, A07302, doi:10.1029/2008JA013073.

Duru, F., D. A. Gurnett, J. D. Winningham, R. A. Frahm, and R. Modolo (2009), A plasma flow velocity boundary at Mars from the disappearance of electron plasma oscillations, *Icarus*, doi:10.1016/j.icarus.2009.04.012, in press.

Elphic, R. C., C. T. Russel, J. G. Luhmann, F. L. Scarf, and L. H. Brace (1981), The Venus ionopause current sheet: Thickness length scale and controlling factors, *J. Geophys. Res.*, *86*(A13), 11,430–11,438, doi:10.1029/JA086iA13p11430.

Fjeldbo, G., W. C. Fjeldbo, and V. R. Eshleman (1966), Models for the atmosphere of Mars based on the Mariner 4 occultation experiment, *J. Geophys. Res.*, *71*, 2307–2316.

Frahm, R. A., et al. (2006), Location of atmospheric photoelectron energy peaks within the Mars environment, *Space Sci. Rev.*, *126*, 389–402, doi:10.1007/s11214-006-9119-5.

Gurnett, D. A., and A. Bhattacharjee (2005), *Introduction to Plasma Physics With Space and Laboratory Applications*, Cambridge Univ. Press, Cambridge, U. K.

Gurnett, D. A., et al. (2005), Radar soundings of the ionosphere of Mars, *Science*, *310*, 1929–1933, doi:10.1126/science.1121868.

Gurnett, D. A., et al. (2008), An overview of radar soundings of the Martian ionosphere from the Mars Express spacecraft, *Adv. Space Res.*, *41*, 1335–1346, doi:10.1016/j.asr.2007.01.062.

Gurnett, D. A., D. D. Morgan, F. Duru, F. Akalin, J. D. Winningham, R. A. Frahm, E. Dubinin, and S. Barabash (2009), Large density fluctuations in the Martian ionosphere as observed by the Mars Express radar sounder, *Icarus*, doi:10.1016/j.icarus.2009.02.019, in press.

Hinson, D. P., G. L. Tyler, L. J. Hollingsworth, and R. J. Wilson (2001), Radio occultation measurements of forced atmospheric waves on Mars, *J. Geophys. Res.*, *106*, 1463–1480, doi:10.1029/2000JE001291.

Kliore, A. J. (1992), Radio occultation observations of the ionospheres of Mars and Venus, in *Venus and Mars, Ionospheres, and Solar Wind Interactions*, *Geophys. Monogr. Ser.*, vol. 66, edited by J. G. Luhmann, M. Tatrallyay, and R. Pepin, pp. 265–276, AGU, Washington, D. C.

Kliore, A., D. L. Cain, G. S. Levy, V. R. Eshleman, G. Fjeldbo, and F. D. Drake (1965), Occultation experiment: Results of the first direct measurement of Mars's atmosphere and ionosphere, *Science*, *149*, 1243–1248, doi:10.1126/science.149.3689.1243.

Knudsen, W. C., K. Spenner, R. C. Whitten, J. R. Spreiter, K. L. Miller, and V. Novak (1979), Thermal structure and major ion composition of the Venus ionosphere: First RPA results from Venus orbiter, *Science*, *203*, 757–763, doi:10.1126/science.203.4382.757.

Luhmann, J. G., and L. H. Brace (1991), Near-Mars space, *Rev. Geophys.*, *29*, 121–140, doi:10.1029/91RG00066.

Morgan, D. D., D. A. Gurnett, D. L. Kirchner, J. L. Fox, E. Nielsen, and J. J. Plaut (2008), Variation of the Martian ionospheric electron density from Mars Express radar sounding, *J. Geophys. Res.*, *113*, A09303, doi:10.1029/2008JA013313.

Nagy, A. F., et al. (2004), The plasma environment of Mars, *Space Sci. Rev.*, *111*, 33–114, doi:10.1023/B:SPAC.0000032718.47512.92.

Ness, N. F., et al. (1999), MGS magnetic fields and electron reflectometer investigation: Discovery of paleomagnetic fields due to crustal remanence, *Adv. Space Res.*, *23*(11), 1879–1886, doi:10.1016/S0273-1177(99)00271-9.

Pätzold, M., S. Tellmann, B. Häusler, D. Hinson, R. Schaa, and G. L. Tyler (2005), A sporadic third layer in the ionosphere of Mars, *Science*, *310*, 837–839, doi:10.1126/science.1117755.

Picardi, G., et al. (2004), MARSIS: Advanced Radar for Subsurface and Ionosphere Sounding, in *Mars Express: A European Mission to the Red Planet*, *Eur. Space Agency Spec. Publ., ESA SP-1240*, 51–70.

Schunk, R. W., and A. F. Nagy (2000), *Ionospheres: Physics, Plasma Physics, and Chemistry*, Cambridge Univ. Press, Cambridge, U. K.

Smith, E. J., L. Davis Jr., P. J. Coleman Jr., and D. E. Jones (1965), Magnetic field measurements near Mars, *Science*, *149*, 1241–1242, doi:10.1126/science.149.3689.1241.

Trotignon, J. G., C. Bertucci, and M. H. Acuña (2006), Martian shock and magnetic pile-up boundary positions and shapes determined from the Phobos 2 and Mars Global Surveyor data sets, *Planet. Space Sci.*, *54*, 357–369, doi:10.1016/j.pss.2006.01.003.

Van Allen, J. A., L. A. Frank, S. M. Krimigis, and H. K. Hillis (1965), Absence of Martian radiation belts and implications thereof, *Science*, *149*, 1228–1233, doi:10.1126/science.149.3689.1228.

Zhang, M. H. G., J. G. Luhmann, and A. J. Kliore (1990), A post-Pioneer Venus reassessment of the Martian dayside ionosphere as observed by radar occultation methods, *J. Geophys. Res.*, *95*, 14,829–14,839, doi:10.1029/JB095iB09p14829.

F. Duru, D. A. Gurnett, G. G. Howes, and D. D. Morgan, Department of Physics and Astronomy, University of Iowa, Iowa City, IA 52242, USA. (firdevs.duru@gmail.com)

R. A. Frahm and J. D. Winningham, Southwest Research Institute, PO Drawer 28510, San Antonio, TX 78228, USA.